

## ON THE ORIENTATION AND MAGNITUDE OF THE BLACK HOLE SPIN IN GALACTIC NUCLEI

M. DOTTI<sup>1,2</sup>, M. COLPI<sup>1,2</sup>, S. PALLINI<sup>1</sup>, A. PEREGO<sup>3</sup>, M. VOLONTERI<sup>4,5</sup>*To appear in ApJ*

## ABSTRACT

Massive black holes in galactic nuclei vary their mass  $M_{\text{BH}}$  and spin vector  $\mathbf{J}_{\text{BH}}$  due to accretion. In this study we relax, for the first time, the assumption that accretion can be either chaotic, i.e. when the accretion episodes are randomly and isotropically oriented, or coherent, i.e. when they occur all in a preferred plane. Instead, we consider different degrees of anisotropy in the fueling, never confining to accretion events on a fixed direction. We follow the black hole growth evolving contemporarily mass, spin modulus  $a$  and spin direction. We discover the occurrence of two regimes. An early phase ( $M_{\text{BH}} \lesssim 10^7 M_{\odot}$ ) in which rapid alignment of the black hole spin direction to the disk angular momentum in each single episode leads to erratic changes in the black hole spin orientation and at the same time to large spins ( $a \sim 0.8$ ). A second phase starts when the black hole mass increases above  $\gtrsim 10^7 M_{\odot}$  and the accretion disks carry less mass and angular momentum relatively to the hole. In the absence of a preferential direction the black holes tend to spin-down in this phase. However, when a modest degree of anisotropy in the fueling process (still far from being coherent) is present, the black hole spin can increase up to  $a \sim 1$  for very massive black holes ( $M_{\text{BH}} \gtrsim 10^8 M_{\odot}$ ), and its direction is stable over the many accretion cycles. We discuss the implications that our results have in the realm of the observations of black hole spin and jet orientations.

*Subject headings:* Black hole physics — Accretion, accretion disks — galaxies: active — galaxies: jets

## 1. INTRODUCTION

Massive black holes (BHs) that inhabit in the nuclei of massive galaxies are described by only two parameters: their mass  $M_{\text{BH}}$  and spin  $\mathbf{J}_{\text{BH}}$ .

Tens of BH masses in quiescent, nearby galaxies have been directly estimated to date studying the dynamics of stars and gas and these masses all fall within  $\gtrsim 10^6 M_{\odot} - 10^{10} M_{\odot}$  (e.g. Gültekin et al. 2009, McConnell et al. 2011 and references therein). Similarly, tens of thousands BH masses in active nuclei have also been estimated using empirical relations, and, while for quasars their median mass is in excess of  $10^8 M_{\odot}$  (e.g., Vestergaard et al. 2008), faint AGN are powered by BHs with masses as small as  $\sim 10^5 M_{\odot}$  (Peterson et al. 2005).

Measurements of the dimensionless spin parameter  $a$  are more controversial. The parameter  $a$  has been recently measured only for few AGNs (e.g. Brenneman & Reynolds 2006; Schmoll et al. 2009; de la Calle Perez et al. 2010; Patrick et al. 2011a,b; Gallo et al. 2011; Brenneman et al. 2011) through X-ray spectroscopy. However, several free parameters enter in the estimate, creating a severe degeneracy problem. For example, different groups obtained different estimates of  $a$  in MCG-6-30-15:  $a > 0.98$  (Brenneman & Reynolds 2006),  $a = 0.86 \pm 0.01$  (de la Calle Perez et al. 2010) and  $a = 0.49^{+0.20}_{-0.12}$  (Patrick et al. 2011a). Even more problematic is the case of NGC

3783, for which different groups found  $a > 0.88$  (Brenneman et al. 2011) and  $a < 0.32$  (Patrick et al. 2011b). Measuring and understanding spins is crucial to assess the cosmic evolution of massive BHs. Firstly, spins affect the accretion-luminosity conversion efficiency; highly spinning BHs can convert up to  $\sim 40\%$  of the accreted matter into radiation, making them more luminous, albeit making their growth slower. Secondly, the spin paradigm assumes that radio jets observed in AGNs are launched by highly spinning BHs (Blandford & Znajek 1977). Lastly, spins dramatically affect the gravitational recoil suffered by the remnant BH after a binary merger. It has in fact been shown that highly spinning BHs can experience kicks up to  $5000 \text{ km s}^{-1}$  depending on their progenitor spin magnitude and orientation (Campanelli et al. 2007; Baker et al. 2008; Herrmann et al. 2007; Schnittman & Buonanno 2007; Lousto & Zlochower 2011; Lousto et al. 2012). These super-kicks are sufficient to eject the remnant from the deepest potential well of the most massive galaxies, with potentially important implications for the occupation fraction of massive BHs in galaxies (Schnittman 2007; Volonteri 2007; Volonteri, Haardt & Gültekin 2008; Volonteri, Gültekin & Dotti 2010).

BH masses and spins are thought to build up through gas accretion and BH mergers, and their history of growth erases the initial values of  $M_{\text{BH}}$  and  $a$ . The main driver of the BH spin evolution is gas accretion (Berti & Volonteri 2008; Fanidakis et al. 2011; Barausse 2012)<sup>6</sup>. Two different accretion scenarios have been proposed to date: (i) *coherent accretion*, in which the BHs accrete gas with a well defined, almost constant, angular momentum direction, and (ii) *chaotic accretion*, in which parcels of gas accrete on the BHs in randomly oriented planes (e.g.

<sup>1</sup> Dipartimento di Fisica G. Occhialini, Università degli Studi di Milano Bicocca, Piazza della Scienza 3, 20126 Milano, Italy  
E-mail: Massimo.Dotti@mib.infn.it

<sup>2</sup> INFN, Sezione di Milano-Bicocca, Piazza della Scienza 3, 20126 Milano, Italy

<sup>3</sup> Department of Physics, University of Basel, Klingenbergstr. 82, 4056 Basel, Switzerland

<sup>4</sup> Astronomy Department, University of Michigan, Ann Arbor 48109, USA

<sup>5</sup> Institut d'Astrophysique de Paris, 98 bis Bd Arago, Paris, 75014, France

<sup>6</sup> With the possible exception of the most massive BHs in massive, gas-poor, low-redshift ellipticals (e.g. Fanidakis et al. 2011).

King et al. 2005; King & Pringle 2006; 2007). The two models result in different BH evolutions and different expected distributions of the spin magnitudes. Coherent accretion keeps on adding angular momentum to the BHs in the same direction and results in very high spins ( $0.8 \lesssim a \lesssim 1$ ) aligned with the angular momentum of the accreting material (e.g. Dotti et al. 2010 and references therein). The chaotic case is more subtle: gas accretion on a rotating BH on a retrograde orbit has a larger last stable orbit than gas with angular momentum aligned with the BH spin. As a consequence, retrograde accreting gas transfers to the BH more (and negative) angular momentum per unit of mass than the prograde. If retrograde and prograde accretion are equally probable (as implicitly assumed in the chaotic scenario), the BH spin  $a$  is biased toward low values ( $0 \lesssim a \lesssim 0.2$ , King, Pringle & Hofmann 2008; Berti & Volonteri 2008).

These two models cover the extreme cases in which the gas either flows from a stable, fixed direction or from fully random directions. In this investigation we relax these extreme and unrealistic assumptions, exploring the evolution of the BH mass and spin vector varying the degree of anisotropy in the fueling process to mimic anisotropies present in the gas in the nuclear regions of active galaxies. We demonstrate how the evolution of the BH spin direction and magnitude is coupled, with the evolution of the spin direction determining the growth or reduction of  $a$ .

The paper is organized as follows: in Section 2 we describe the gas dynamics and introduce the equations of evolution for the mass and spin of the accreting BHs; in Section 3 we discuss our results; in Section 4 we summarize the results and in Section 5 we discuss the potential implications of our study on the growth of BHs and on jet formation.

## 2. METHODOLOGY

We follow individual BH histories by tracing the evolution of the black hole mass  $M_{\text{BH}}$  and angular momentum vector  $\mathbf{J}_{\text{BH}} = (aGM_{\text{BH}}^2/c)\hat{\mathbf{J}}_{\text{BH}}$ , where we denote with  $0 \leq a \leq 1$  the dimensionless spin parameter and with  $\hat{\mathbf{J}}_{\text{BH}}$  the spin orientation. A single history is a sequence of multiple accretion episodes during which  $M_{\text{BH}}$ ,  $a$  and  $\hat{\mathbf{J}}_{\text{BH}}$  vary upon time  $t$  according to the recipes described below.

### 2.1. The accretion disk properties

In every single accretion episode the BH is assumed to be surrounded by a stationary geometrically thin, optically thick  $\alpha$ -disk (Shakura & Sunyaev 1973). The accretion rate  $\dot{M}$  is expressed in terms of the Eddington factor  $f_{\text{Edd}}$ , and the accretion efficiency  $\eta$  (which is a function of  $a$ , Bardeen 1970; Bardeen et al. 1972) according to the relation

$$\dot{M} = \frac{f_{\text{Edd}}}{\eta} \frac{M_{\text{BH}}}{\tau_{\text{S}}} = 2 \times 10^{-2} M_{\text{BH},6} \left( \frac{f_{\text{Edd}}}{\eta_{0.1}} \right) M_{\odot} \text{ yr}^{-1}, \quad (1)$$

where  $\eta_{0.1}$  is the efficiency in units of 0.1,  $M_{\text{BH},6}$  the BH mass in units of  $10^6 M_{\odot}$ ,  $\tau_{\text{S}} = \sigma_{\text{T}} c / (4\pi G m_{\text{p}}) = 4.5 \times 10^8$  yr,  $\sigma_{\text{T}}$  is the Thomson cross-section, and  $m_{\text{p}}$  is the proton mass.

We set the total mass of the disk  $m_{\text{disk}}$  at each accretion episode equal to the minimum between (i)  $m_{\text{cloud}}$ , i.e. the mass of a gas cloud that we assume to be available in a single feeding episode, and (ii) the self-gravitating mass  $m_{\text{sg}}$ , the largest for an  $\alpha$ -disk to be stable against fragmentation by its own self gravity (e.g. Kolykhalov & Sunyaev 1980). The mass  $m_{\text{cloud}}$  is taken to be a constant, i.e. independent of the BH mass, and carries two possible values  $10^4 M_{\odot}$  and  $10^5 M_{\odot}$ . Within a given accretion history, i.e. over the whole BH's life, the mass of the cloud is kept fixed at either  $10^4 M_{\odot}$  and  $10^5 M_{\odot}$ . The self-gravitating mass  $m_{\text{sg}}$ , for the  $\alpha$ -disk, is computed from the distance  $R_{\text{disk,sg}}$  at which the Toomre parameter  $Q \sim c_{\text{s}} \Omega / \pi G \Sigma \lesssim 1$ , so that at radii  $R < R_{\text{disk,sg}}$  the disk is stable (where  $c_{\text{s}}$  is the central sound speed,  $\Omega$  the Keplerian angular velocity of fluid elements in the disk, and  $\Sigma$  the surface mass density). This yields

$$\frac{R_{\text{disk,sg}}}{R_{\text{G}}} \approx 10^5 \alpha_{0.1}^{28/45} M_{\text{BH},6}^{-52/45} \left( \frac{f_{\text{Edd}}}{\eta_{0.1}} \right)^{-22/45} \quad (2)$$

where  $\alpha_{0.1} = \alpha/0.1$  is the radial shear viscosity parameter in units of 0.1, and  $R_{\text{G}}$  the BH gravitational radius  $R_{\text{G}} = 2GM_{\text{BH}}/c^2$ . Using the solution for the surface density in the external region of the disk,  $\Sigma(R) = \Sigma_0 (R/R_{\text{G}})^{-3/4}$  with

$$\Sigma_0 = 7 \times 10^7 \alpha_{0.1}^{-4/5} M_{\text{BH},6}^{19/20} \left( \frac{f_{\text{Edd}}}{\eta_{0.1}} \right)^{7/10} \text{ g cm}^{-2}, \quad (3)$$

the self-gravitating disk mass reads

$$m_{\text{sg}} \approx (8\pi/5) R_{\text{G}}^2 \Sigma_0 (R_{\text{disk,sg}}/R_{\text{G}})^{5/4}, \quad (4)$$

and accordingly

$$m_{\text{sg}} \approx 2 \times 10^4 \alpha_{0.1}^{-1/45} \left( \frac{f_{\text{Edd}}}{\eta_{0.1}} \right)^{4/45} M_{\text{BH},6}^{34/45} M_{\odot}. \quad (5)$$

When the disk mass equals  $m_{\text{cloud}}$ , the outer radius  $R_{\text{disk,cl}}$  is computed as the integral over the surface density yielding,

$$\frac{R_{\text{disk,cl}}}{R_{\text{G}}} \approx 4 \times 10^4 \left( \frac{m_{\text{cloud}}}{10^4 M_{\odot}} \right)^{4/5} \alpha_{0.1}^{16/25} M_{\text{BH},6}^{-44/25} \left( \frac{f_{\text{Edd}}}{\eta_{0.1}} \right)^{-14/25}. \quad (6)$$

Very massive BHs can stabilize huge accretion disks against their own self-gravity. As an example,  $m_{\text{sg}} \lesssim 10^7 M_{\odot}$  for  $M_{\text{BH}} \sim 10^9 M_{\odot}$ . Such a large reservoir of mass may not be available in a single accretion episode. In fact observations indicate that the mass fraction of cold gas relative to stars decreases with increasing galaxy mass (e.g. di Serego Alighieri et al. 2007, Catinella et al. 2010). To avoid unrealistically massive accretion episodes, we adopt the following criterion: if  $m_{\text{cloud}} > m_{\text{sg}}$ , the disk around the accreting BH is truncated at  $R_{\text{disk,sg}}$  and has mass  $m_{\text{sg}}$ ; by contrast if  $m_{\text{cloud}} < m_{\text{sg}}$ , the disk is truncated at  $R_{\text{disk,cl}}$  and has mass  $m_{\text{cloud}}$ . Thus for a given value of  $m_{\text{cloud}}$ , representing the mass reservoir in a single accretion episode, there exists a characteristic BH mass  $M_{\text{BH}}^{\text{crit}}$  for which  $m_{\text{sg}} = m_{\text{cloud}}$ :

$$M_{\text{BH},6}^{\text{crit}} = 0.4 \alpha_{0.1}^{1/34} \left( \frac{f_{\text{Edd}}}{\eta_{0.1}} \right)^{-2/17} \left( \frac{m_{\text{cloud}}}{10^4 M_{\odot}} \right)^{45/34}. \quad (7)$$

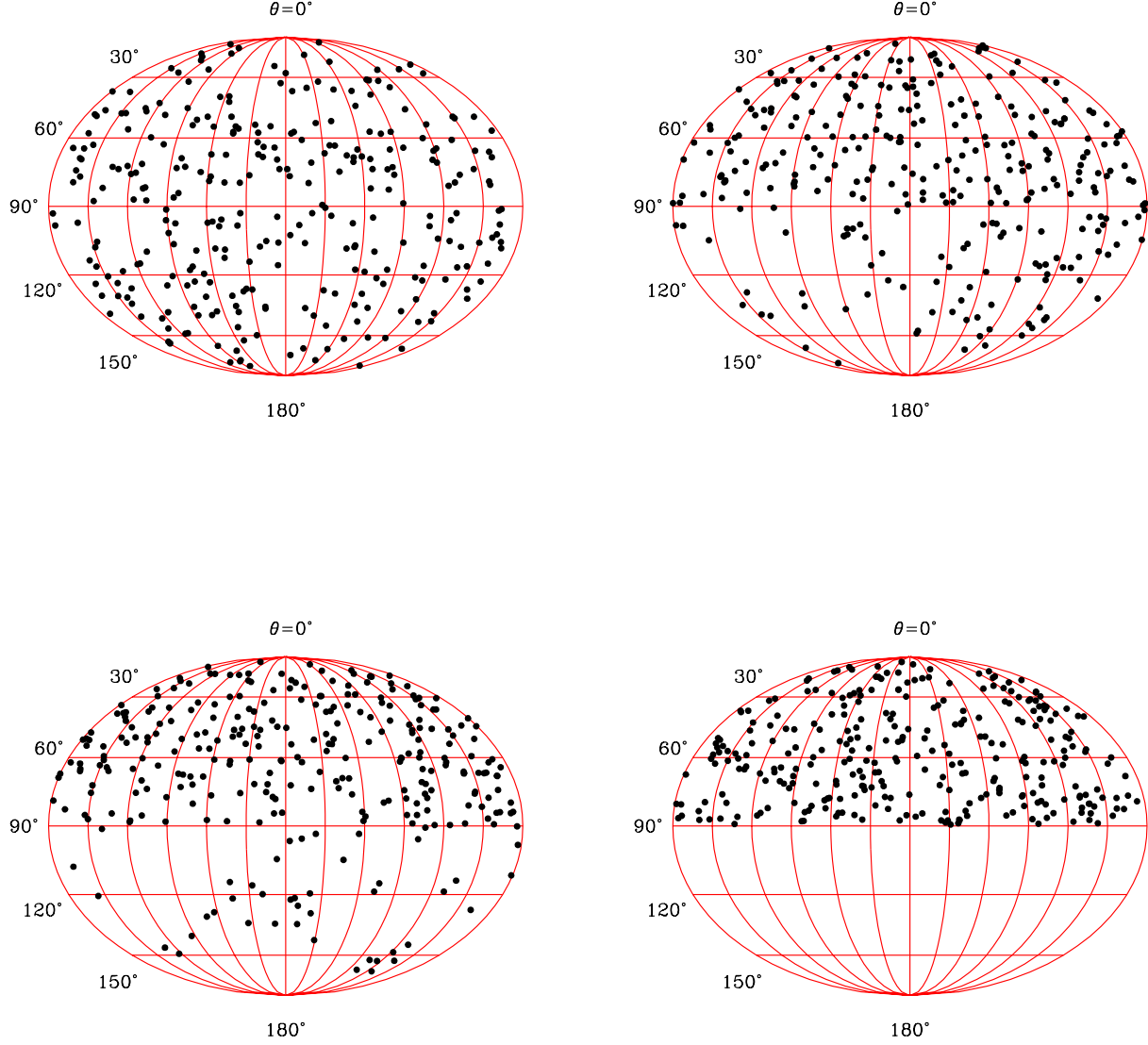


FIG. 1.— Distribution of the directions of  $\hat{\mathbf{J}}_{\text{disk}}$  for different degrees of anisotropy. Top-left panel refers to the case of complete isotropy ("chaotic" accretion,  $F = 0.5$ ). Top-right, bottom-left, and bottom-right panels refer to accretion with levels of anisotropy  $F = 0.25$ ,  $0.125$  and  $0$ , respectively.

The mass during a single accretion episode is consumed over a timescale  $\tau_{\text{acc}}$  that in the two regimes (when the BH mass is below or above  $M_{\text{BH}}^{\text{crit}}$  respectively) reads:

$$\tau_{\text{acc,sg}} = \frac{m_{\text{sg}}}{\dot{M}} \approx 10^6 \alpha_{0.1}^{-1/45} M_{\text{BH},6}^{-11/45} \left( \frac{f_{\text{Edd}}}{\eta_{0.1}} \right)^{-14/45} \text{yr}, \quad (8)$$

$$\tau_{\text{acc,cl}} = \frac{m_{\text{cloud}}}{\dot{M}} \approx 5 \times 10^5 \frac{m_{\text{cloud}}}{10^4 M_{\odot}} M_{\text{BH},6}^{-1} \left( \frac{f_{\text{Edd}}}{\eta_{0.1}} \right)^{-1} \text{yr}. \quad (9)$$

## 2.2. The black hole and the disk angular momenta

The ratio of the angular momentum carried by the disk and the angular momentum of the black hole is the main driver of how much an accretion episode, and a series of accretion episodes can modify the direction and magnitude of a BH spin. The  $\alpha$ -disk carries an angular momentum  $\mathbf{J}_{\text{disk}}$  obtained integrating over all annuli the disk angular momentum surface density  $\mathbf{L}(R) = L(R)\hat{\mathbf{l}}(R)$ , where  $\hat{\mathbf{l}}(R)$  is the local orientation of  $\mathbf{L}$  in the disk, and  $L(R) = \Sigma(R)\Omega(R)R^2$ . Following Perego et al. (2009; Perego09 hereafter),

$$J_{\text{disk}}(R) \propto \dot{M} \sqrt{GM_{\text{BH}}} R^{7/4}. \quad (10)$$

The ratio between the angular momentum of the disk and BH reads:

$$\frac{J_{\text{disk}}(R_{\text{disk,sg}})}{J_{\text{BH}}} \sim 7.3 \alpha_{0.1}^{13/45} \left( \frac{f_{\text{Edd}}}{\eta_{0.1}} \right)^{-7/45} M_{\text{BH},6}^{-37/45} a^{-1}. \quad (11)$$

Since  $J_{\text{disk}} \propto R^{7/4}$ , disks that are not truncated by self-gravity carry an angular momentum smaller by a factor  $(R_{\text{disk,cl}}/R_{\text{disk,sg}})^{7/4}$  than disks with mass  $m_{\text{sg}}$ , and this will play a role in modeling the BH history.

The orientation of  $\mathbf{J}_{\text{disk}}$ , denoted as  $\hat{\mathbf{J}}_{\text{disk}}$ , is determined mainly by the angular momentum in the outermost region of the disk.  $\hat{\mathbf{J}}_{\text{disk}}$  is uncorrelated with the BH spin direction  $\hat{\mathbf{J}}_{\text{BH}}$  at the onset of any accretion episode. Hereon, disk orientation is described in terms of the polar angle  $\theta_{\text{disk}}$  between  $\hat{\mathbf{J}}_{\text{disk}}$  and a fixed reference direction, i.e. the unit vector  $\mathbf{e}_z$  in our spherical coordinate reference system:  $\theta_{\text{disk}} = \cos^{-1}(\hat{\mathbf{J}}_{\text{disk}} \cdot \mathbf{e}_z)$ .

The orientation of the accretion disk is selected through Montecarlo sampling. We follow four different prescriptions that correspond to different degrees of anisotropy in the BH fuelling process. In the first,  $\hat{\mathbf{J}}_{\text{disk}}$  is distributed at random. This corresponds to a uniform distribution for the azimuthal angle  $\phi_{\text{disk}}$  and to a distribution proportional to  $\sin \theta$  for the polar angle  $\theta_{\text{disk}}$ . In this particular case, the fraction  $F$  of accretion events with  $\theta_{\text{disk}} > 90^\circ$  is 0.5. The other three cases are constructed following initially the same procedure, but inverting at random the sign of  $\theta_{\text{disk}}$  to build three distributions with  $F = 0.25$ ,  $F = 0.125$ , and  $F = 0$ .  $F = 0.25$  corresponds to a distribution with three times more events in the “northern hemisphere” ( $\theta_{\text{disk}} < 90^\circ$ ) than in the “southern hemisphere” ( $\theta_{\text{disk}} > 90^\circ$ ),  $F = 0.125$  corresponds to a distribution with a north-to-south events ratio of seven, and the distribution with  $F = 0$  has no events in the southern hemisphere. Figure 1 shows the distributions of  $\hat{\mathbf{J}}_{\text{disk}}$  for the four values of  $F$  considered. Note that the  $F = 0.5$  case is exactly what is assumed in the standard “chaotic accretion” scenario.  $F = 0$ , on the other hand, does not correspond to “coherent accretion”, but it mimics accretion through disk clouds that are distributed isotropically but that share a common sense of rotation.  $F = 0$  corresponds to a 3D-dispersion to rotation velocity ratio  $\sigma/v_{\text{rot}} \lesssim 1$  for the gas fuelling the BH.

The direction of the BH spin vector  $\hat{\mathbf{J}}_{\text{BH}}$ , initially selected at random, is followed by tracking the BH spin and accretion history and by recording the values of  $a$ ,  $\hat{\mathbf{J}}_{\text{BH}}$  and  $M_{\text{BH}}$  at the end of each accretion episode. Hereon we denote with  $\theta_{\text{BH}}$  the polar angle of  $\hat{\mathbf{J}}_{\text{BH}}$  with  $\mathbf{e}_z$ , i.e.  $\theta_{\text{BH}} = \cos^{-1}(\hat{\mathbf{J}}_{\text{BH}} \cdot \mathbf{e}_z)$ . The BH spin vector can point in all directions, and  $\hat{\mathbf{J}}_{\text{BH}}$  as well as  $\hat{\mathbf{J}}_{\text{disk}}$  are referred to the reference frame of the galaxy defined by  $\mathbf{e}_z$ .

### 2.3. $a$ , $\hat{\mathbf{J}}_{\text{BH}}$ and $M_{\text{BH}}$ on a history path

At the onset of any accretion episode the BH spin vector  $\mathbf{J}_{\text{BH}}$  is generally misaligned with respect to the direction of the accretion disk  $\hat{\mathbf{J}}_{\text{disk}}$ . In high viscosity  $\alpha$ -disks, this configuration is unstable and evolving into a lower energy state. There is an early phase in which gravito-magnetic torques exerted by the spinning BH on

disk’s fluid elements cause the disk to warp on a timescale  $\tau_{\text{warp}}$  (Bardeen & Petterson 1975); the second phase is the alignment phase, i.e. a change in the orientation of the BH spin over a longer time.

In the early phase, the spinning BH induces Lense-Thirring precession of the orbital plane of disk’s fluid elements: precession of the plane occurs at a frequency  $\omega_{\text{prec}} = (2G/c^2)J_{\text{BH}}/R^3 = (2G/c)aM_{\text{BH}}^2/R^3$ , so that fluid elements closer to the BH precess faster. Close to the BH, their orbital plane tends to align (or anti-align if counter-rotating) parallel to the BH spin direction  $\hat{\mathbf{J}}_{\text{BH}}$ , on times shorter at shorter radii, so that the perturbation diffuses radially outwards, on a timescale  $\tau_{\text{warp}} \sim R^2/\nu_2$ , where  $\nu_2$  is the vertical shear viscosity. The disk is maximally warped at  $R_{\text{warp}}$ , corresponding to the distance where the warp-diffusion timescale becomes comparable or shorter than the precession time  $\omega_{\text{prec}}^{-1}$ :

$$\frac{R_{\text{warp}}}{R_G} \sim \frac{4GJ_{\text{BH}}}{\nu_2 c^2 R_G} \sim 500 \alpha_{0.1}^{24/35} f_{\nu_2}^{4/7} M_{\text{BH},6}^{4/35} \left( \frac{f_{\text{Edd}}}{\eta_{0.1}} \right)^{-\frac{6}{35}} a^{4/7}, \quad (12)$$

where  $\nu_2 \sim \alpha_2 c_s H$  with  $\alpha_2 \approx f_{\nu_2}/(2\alpha)$  (Lodato & Pringle 2007; Perego09 for details)  $R_{\text{warp}}$  indicates the region in the inner disk where the fluid elements align or antialign with  $\hat{\mathbf{J}}_{\text{BH}}$ . At  $R \sim R_{\text{warp}}$  the warp timescale is

$$\tau_{\text{warp}} \sim 35 \alpha_{0.1}^{72/35} f_{\nu_2}^{-12/7} M_{\text{BH},6}^{47/35} \left( \frac{f_{\text{Edd}}}{\eta_{0.1}} \right)^{-\frac{18}{35}} a^{5/7} \text{ yr}. \quad (13)$$

Since the warp timescale is shorter than the viscous timescale at all annuli, the deformation diffuses more rapidly outwards than the inward radial drift motion so that the deformed disk attains an equilibrium profile, and the shape of the perturbation is stationary (Martin et al. 2007).

The warped disk (in the small deformation approximation) is described by an equilibrium surface density  $\Sigma(R)$  and a velocity  $\Omega(R)$  close to that of an unperturbed Keplerian disk, plus a deformation in the local angular momentum vector (per unit surface area)  $\mathbf{L} = L(R)(\hat{l}_x, \hat{l}_y, \hat{l}_z)$  (with  $\hat{\mathbf{l}}$  a unit vector in the direction of  $\mathbf{L}$ ; we defer to Perego09 for details). Angular momentum conservation then imposes the spinning BH to precess and align relative to the total angular momentum  $\mathbf{J}_{\text{tot}} = \mathbf{J}_{\text{disk}} + \mathbf{J}_{\text{BH}}$ . During individual accretion episodes at a rate  $\dot{M}$ , the BH mass increases according to:

$$\frac{dM_{\text{BH}}}{dt} = (1 - \eta)\dot{M}c^2 = (1 - \eta) \left( \frac{f_{\text{Edd}}}{\eta} \right) \frac{M_{\text{BH}}}{\tau_S}, \quad (14)$$

with an  $e$ -folding timescale

$$\tau_{M_{\text{BH}}} \sim \frac{\eta \tau_S}{(1 - \eta)f_{\text{Edd}}} \sim 5 \times 10^7 \frac{\eta_{0.1}}{(1 - \eta_{0.1})f_{\text{Edd}}} \text{ yr}. \quad (15)$$

The BH angular momentum vector evolves according to

$$\frac{d\mathbf{J}_{\text{BH}}}{dt} = \dot{M} \frac{GM_{\text{BH}}}{c} \Lambda_{\text{isco}} \hat{\mathbf{l}}(R_{\text{ISCO}}) + \frac{4\pi G}{c^2} \int_{\text{disk}} \frac{\mathbf{L} \times \mathbf{J}_{\text{BH}}}{R^2} dR \quad (16)$$

where the first term in equation (15) describes the change in the spin modulus  $a$  due to the transfer of angular

momentum per unit mass at the innermost stable circular orbit  $R_{\text{ISCO}}$  (where  $\Lambda(R_{\text{ISCO}})$  is a known dimensionless function of  $a$ ). Gravito-magnetic coupling in the inner region of the precessing disk ensures that the direction of  $\hat{\mathbf{l}}(R_{\text{ISCO}})$  is parallel or anti-parallel to  $\hat{\mathbf{J}}_{\text{BH}}$ .

The second term of equation (16) describes the change in the BH spin orientation which tends to reduce the degree of misalignment between the disk and the BH spin (Perego09; Scheuer & Feiler 1996). An intuitive explanation for the alignment is as follows. The warping of the disk results always in a either aligned or antialigned inner part of the accretion disk, due to the BH metric. On the other hand, since the frequency of the Lense-Thirring precession decreases with radius, the outer part of the accretion disk can effectively be considered unperturbed (this corresponds to the Newtonian limit for the accretion disk), and there exists a region (near the so called warp radius) where the local disk angular momentum unit vector is strongly misaligned both with the spin and disk's angular momentum at far distances (in the unperturbed disk). In other words, gas moving from the unperturbed outer region into the innermost region modifies its angular momentum direction. As a consequence, the BH has to (at least partially) align with the direction of the angular momentum of the outer accretion disk to ensure conservation of the total angular momentum, and to compensate the "loss/change" of angular momentum in the warp region. The alignment effect on the BH spin due to the cumulative torques exerted by a mass distribution does not necessarily require the presence of viscosity. The same alignment can be induced (under some conditions) by the spin orbit interaction between the BH and a rotating stellar cusp (see Merritt & Vasiliev 2012). Viscosity guarantees alignment of the inner disk region and thus guarantees the occurrence of a stationary warp region in the disk causing the torquing of the BH and in turn spin alignment. From equation (16), we can infer an evolution equation for the spin modulus

$$\frac{da}{dt} = \left[ \frac{\Lambda(R_{\text{ISCO}})}{\eta} - 2a \left( \frac{1}{\eta} - 1 \right) \right] \frac{f_{\text{Edd}}}{\tau_{\text{S}}}. \quad (17)$$

Equation (17) shows that changes in the spin modulus  $a$  typically occur on the timescale  $\tau_{\text{spin}} = a/\dot{a}$  comparable to  $\tau_{M_{\text{BH}}}$  (eq. 15). As shown in Bardeen (1970), a non-spinning BH ( $a = 0$ ) is spun up to an extreme Kerr BH ( $a = 1$ ) after having accreted a mass  $\sqrt{6}M_{\text{BH}}$ . The timescale of the alignment process (16) is much shorter. The peak of the torque perpendicular to the BH spin (that responsible for the evolution of the spin direction) is maximal at the warp radius (where the direction of the angular momentum of the gas in the disk changes). The warp radius is considerably larger than the last stable orbit, so the angular momentum per unit of mass of the gas at the warp radius is much larger than that at the ISCO. As a consequence, the torque exerted onto the BH responsible for the evolution of its direction is considerably larger than that responsible for the spin magnitude evolution. Consequently, this results in a shorter timescale for the spin alignment with respect to that associated to the spin magnitude evolution.

Equations (14) and (16) are integrated considering initial BH masses of  $M_{\text{BH},0} = 10^5 M_{\odot}$ , and arbitrary initial spin moduli ( $a_0$ ) and orientations;  $f_{\text{Edd}}$  that en-

ters all timescales can be considered as a scaling parameter so that smaller values of  $f_{\text{Edd}}$  imply longer times. In the calculation we fix  $f_{\text{Edd}} = 0.1$ . According to equation (16), if the disk angular momentum contributes most to  $\mathbf{J}_{\text{tot}}$ , the BH spin-disk orientation angle  $\zeta_{\text{BH,disk}} = \cos^{-1}(\hat{\mathbf{J}}_{\text{BH}} \cdot \hat{\mathbf{J}}_{\text{disk}})$  reduces to zero (i.e. full alignment even starting with  $\zeta_{\text{BH,disk}} = 180^\circ$ ) on a timescale

$$\tau_{\text{al}} \sim 10^5 \alpha_{0.1}^{58/35} f_{\nu_2}^{-5/7} M_{\text{BH},6}^{-2/35} \left( \frac{f_{\text{Edd}}}{\eta_{0.1}} \right)^{-\frac{32}{35}} a^{5/7} \text{yr} \quad (18)$$

(Martin et al. 2007; Lodato & Pringle 2006; Perego09). The timescales  $\tau_{\text{warp}}$  and  $\tau_{\text{al}}$  depend on  $a$  and  $M_{\text{BH}}$  explicitly, and the following inequalities hold

$$\tau_{\text{warp}} < \tau_{\text{al}} < \tau_{\text{acc}} < \tau_{M_{\text{BH}}} \sim \tau_{\text{spin}}. \quad (19)$$

In our study, we integrate the BH spin evolution equation over timesteps  $\delta t$  that are  $\tau_{\text{warp}} < \delta t < \tau_{\text{al}}$  tracing contemporarily the change in  $a$ ,  $\hat{\mathbf{J}}_{\text{BH}}$  and  $M_{\text{BH}}$ . We notice that as  $\tau_{\text{spin}} > \tau_{\text{al}}$ , the spin orientation changes rapidly with time, so that we can exclude the possibility that retrograde accretion reduces  $a$  to 0 before re-increasing it to 1. The rapid change in  $\hat{\mathbf{J}}_{\text{BH}}$  compared to the change in  $a$ , favors conditions of prograde accretion episodes, even starting from retrograde conditions.

The progressive increase in  $M_{\text{BH}}$  during accretion episodes with constant  $m_{\text{disk}} = m_{\text{cloud}}$  (when  $M_{\text{BH}} > M_{\text{BH}}^{\text{crit}}$ ) implies the formation of an accretion disk with  $m_{\text{disk}}/M_{\text{BH}}$  always decreasing. Thus the disks that form during single accretion episodes are progressively smaller and carry less angular momentum relative to the BH. Under these circumstances and depending on  $a$ , the dimensionless ratio  $J_{\text{disk}}/J_{\text{BH}} \lesssim 1$ , and the gravito-magnetic BH-disk coupling has little influence on the BH spin direction. At even larger masses (already in the regime where  $J_{\text{disk}}/J_{\text{BH}} < 1$ ) the warp radius  $R_{\text{warp}}$  may rise above  $\gtrsim R_{\text{disk}}$  depending on  $a$ , and equation (16) becomes invalid (Martin et al. 2007). This transition occurs when  $M_{\text{BH},6} > M_{\text{BH},6}^{\text{warp}}$ , where

$$M_{\text{BH},6}^{\text{warp}} \approx 10 \left( \frac{m_{\text{cloud}}}{10^4 M_{\odot}} \right)^{35/82} \alpha_{0.1}^{-1/41} a^{-25/82} \left( \frac{f_{\text{Edd}}}{\eta_{0.1}} \right)^{-\frac{17}{82}}. \quad (20)$$

Under these circumstances, we assume that in any single event  $\mathbf{J}_{\text{BH}}$  aligns instantaneously to the direction of the total angular momentum  $\mathbf{J}_{\text{tot}}$  (King et al. 2005). The re-orientation of  $\mathbf{J}_{\text{BH}}$  is rather small, since in this regime the BH spin is quite close to the total angular momentum already at the beginning of every individual accretion episode ( $\mathbf{J}_{\text{tot}}$  is in fact dominated by  $\mathbf{J}_{\text{BH}}$ ).  $\mathbf{J}_{\text{disk}}$  instead undergoes a fast and significant re-orientation, and is either aligned or antialigned with respect to  $\mathbf{J}_{\text{BH}}$  depending on the initial angle of relative misalignment ( $\zeta_{\text{BH,disk}}$ ) and the  $J_{\text{disk}}/J_{\text{BH}}$  ratio. The two angular momenta are aligned if  $\cos(\zeta_{\text{BH,disk}}) > -J_{\text{disk}}/2J_{\text{BH}}$  (or counter-aligned when the opposite inequality holds; King et al. 2005; Lodato & Pringle 2006). The BH mass and spin parameter are then evolved according to equation (14) and (17).

To summarize, our procedure leads to the following sequence:

- The disk mass is the minimum between the cloud mass

and the self-gravitating mass,  $m_{\text{disk}} = \min(m_{\text{cloud}}, m_{\text{sg}})$ . The transition between the two phases occurs when the BH mass reaches the value  $M_{\text{BH},6}^{\text{crit}}$  given by equation (7); then the disk contains the whole cloud mass.

- Up until  $M_{\text{BH},6} < M_{\text{BH},6}^{\text{warp}}$ , we follow the spin-disk alignment as a function of time by solving for equation (16). Here,  $M_{\text{BH},6}^{\text{warp}}$  is given by equation (20). Above this mass the disk is assumed to be aligned or anti-aligned with the angular momentum of the BH, depending on the initial angle of relative misalignment.

Therefore, three regimes exist,  $M_{\text{BH},6} < M_{\text{BH},6}^{\text{crit}}$ ;  $M_{\text{BH},6}^{\text{crit}} < M_{\text{BH},6} < M_{\text{BH},6}^{\text{warp}}$ , and  $M_{\text{BH},6} > M_{\text{BH},6}^{\text{warp}}$ . While the switch between the first and second regime depends only on the properties of the gas fuelling the BH, the switch between the second and third regime depends also on the BH spin, and this threshold mass, therefore, depends on the whole growth history of the BH, i.e., how it gained its spin. We anticipate that, regardless of the regime, the important parameter that determines BH spin evolution is the ratio  $J_{\text{disk}}/J_{\text{BH}}$ , as previously discussed.

### 3. RESULTS

Figure 2 shows the evolution of the ratio between  $J_{\text{disk}}$  and  $J_{\text{BH}}$  as a function of the BH mass, for accretion histories that differ in the value of  $m_{\text{cloud}}$  and of the anisotropy parameter  $F$ .

As discussed in the previous section we can distinguish an early phase (I) during which the accretion disks carry a large angular momentum, and a second phase (II) where the opposite holds. During phase I, the disks are initially truncated by their own self-gravity and their mass is determined by the BH mass. As the BH grows in mass the disks carry the cloud mass  $m_{\text{cloud}}$ . This transition occurs at  $M_{\text{BH}}^{\text{crit}}$  and is visible as a knee in the  $J_{\text{disk}}/J_{\text{BH}}$  versus BH mass diagram. During phase II, disks are tiny ( $R_{\text{warp}} > R_{\text{disk}}$ ) and there is the switch between the two prescriptions for the BH spin evolution. This occurs around a few  $10^7 M_{\odot}$  and is highlighted as a red shaded area in each panel. The upper left and right panels refer to the isotropic case ( $F = 0.5$ ) with a maximum mass per accretion event  $m_{\text{cloud}} = 10^4 M_{\odot}$  and  $10^5 M_{\odot}$ , respectively. The minimum value of  $J_{\text{disk}}/J_{\text{BH}}$  for the two cases is between  $10^{-2} - 10^{-3}$  and is attained when  $M_{\text{BH}} \gtrsim 10^9 M_{\odot}$ . Similar results are found for different values of the anisotropy parameter, as shown in the bottom panels for  $m_{\text{cloud}} = 10^5 M_{\odot}$ , assuming  $F = 0.25$  and 0 respectively. Notice that in these cases  $J_{\text{disk}}/J_{\text{BH}}$  drops below  $10^{-3}$  for very large masses and this reflects the large spin carried by these BHs. For anisotropic cases ( $F = 0.25; 0$ ) the massive BHs tend to align their spins with the average angular momentum of the gas reservoir, as will be discussed in section 3.1. This results in an higher fraction of prograde accretion events, and, as a consequence, in a higher  $J_{\text{BH}}$ . A detailed description of the evolution in direction and magnitude of  $a$  is presented in the next two sections.

#### 3.1. Evolution of the BH spin direction

The BH spin orientation in a fixed reference frame is defined by two angles, the polar angle  $\theta_{\text{BH}}$ , and the azimuthal angle  $\phi_{\text{BH}}$ . Figure 3 shows, as an example, the

evolution of  $\theta_{\text{BH}}$  as a function of the BH mass for different accretion histories with  $F = 0.5$  (upper panels) 0.25 and 0 (lower left and right panels respectively), and cloud masses  $m_{\text{cloud}} = 10^4 M_{\odot}$  (upper left panel), and  $10^5 M_{\odot}$  (other panels). In case of perfect isotropy in the BH fueling ( $F = 0.5$ ; upper panels in Figure 2), the lack of any preferential direction results in an unbiased random walk of the BH spin direction. This can be quantitatively viewed by plotting the distributions of  $\theta_{\text{BH}}$  and  $\phi_{\text{BH}}$  averaged over 500 accretion histories extracted at random. In the upper panels of Figure 4 we show the distribution of the two angles for the isotropic case for BHs in the mass interval  $10^5 M_{\odot} - 10^6 M_{\odot}$  (green, long dot-dashed line),  $10^6 M_{\odot} - 10^7 M_{\odot}$  (purple, short dot-dashed line),  $10^7 M_{\odot} - 10^8 M_{\odot}$  (red, long dashed line),  $10^8 M_{\odot} - 10^9 M_{\odot}$  (blue, short dashed line) and  $> 10^9 M_{\odot}$  (black, solid line). It is clear that both distributions are consistent with isotropy.

The lower-left panel of Figure 3 refers to the case when  $F = 0.25$ , corresponding to 3/4 of the accretion episodes having the disk angular momentum confined in the northern hemisphere. The behavior of  $\theta_{\text{BH}}$  differs in the two accretion phases (described in the previous section). When  $J_{\text{disk}}/J_{\text{BH}} > 1$  (for masses  $M_{\text{BH}} \lesssim$  few  $10^7 M_{\odot}$ ) the spin orientation aligns significantly with the angular momentum of *each accretion episode*, thus changing erratically over the full range ( $0, 180^\circ$ , despite the fact that the mean is less than  $90^\circ$ ). By contrast, during phase II ( $J_{\text{disk}}/J_{\text{BH}} < 1$ ) the spin tends to align with the *average angular momentum* of the accreting material. In this phase the BH spin slightly tilts toward the direction of the angular momentum of each accreting cloud. The sequence of accretion episodes results in a random walk biased toward the direction of the average angular momentum of the inflow. This trend is illustrated in the two middle panels of Figure 4. While  $\phi_{\text{BH}}$  retains a flat distribution, the distribution of  $\theta_{\text{BH}}$  covers the full  $[0, 180^\circ]$  range for small BH masses, with a 3 times higher probability of  $\theta_{\text{BH}} < 90^\circ$ . For higher masses (i.e. during phase II), the distribution of  $\theta_{\text{BH}}$  shifts toward lower angles, being confined below  $\sim 60^\circ$  for  $M_{\text{BH}} \gtrsim 10^8 M_{\odot}$ . Similarly, for the most anisotropic case considered here ( $F = 0$ ), the BH spin is confined within a solid angle that decreases with increasing BH mass (see the lower right panel of Figure 3 and the lower two panels of Figure 4). For the very massive BHs ( $M_{\text{BH}} > 10^9 M_{\odot}$ ),  $\hat{J}_{\text{BH}}$  is nearly constant, demonstrating the stability of the spin direction even during substantial increase in mass (from  $10^9$  to  $5 \times 10^9 M_{\odot}$ ).

In summary, we show that for small BH masses ( $M_{\text{BH}} \lesssim 10^7 M_{\odot}$ ) the BH spin always aligns to the disk angular momentum in every single accretion episode, and can be substantially misaligned relatively to the average of the angular momenta of the disks. For  $M_{\text{BH}} \gtrsim 10^7 M_{\odot}$ , a single accretion episode does not modify significantly the BH spin direction. In this regime, the BH spin aligns with the average direction of the angular momentum of the accreting material, with a degree of alignment that increases with increasing anisotropy in the fueling process.

#### 3.2. Evolution of the BH spin magnitude $a$

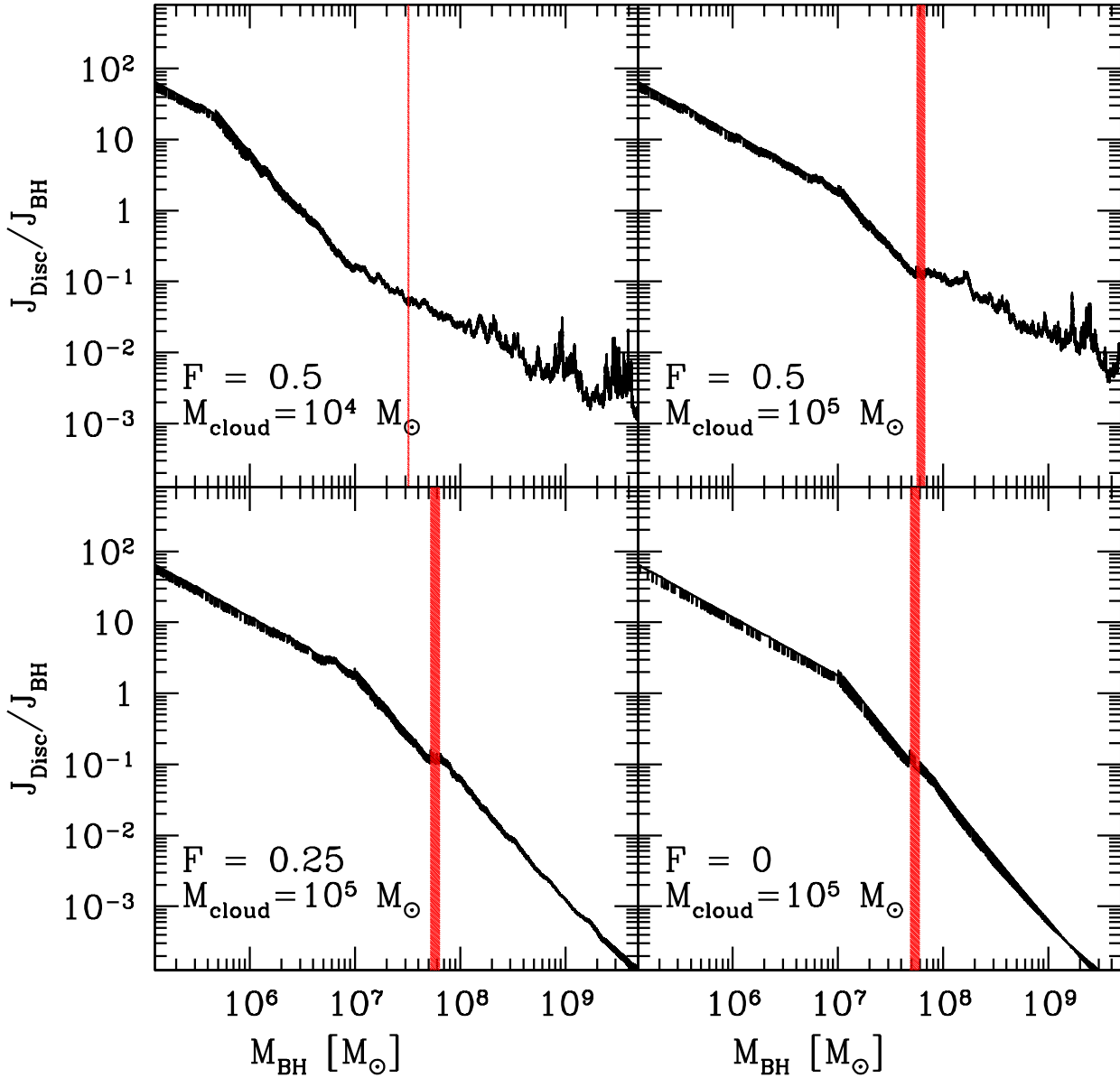


FIG. 2.— Ratio between the total angular momentum of the accretion disk  $\mathbf{J}_{\text{disc}}$  and the BH spin  $\mathbf{J}_{\text{BH}}$ , as a function of the BH mass  $M_{\text{BH}}$ , along an accretion history. The upper left panel refers to the isotropic case ( $F = 0.5$ ) with a maximum mass per accretion event  $m_{\text{cloud}} = 10^4 M_{\odot}$ . The results in the upper right, lower left and lower right panels assume  $m_{\text{cloud}} = 10^5 M_{\odot}$  and  $F = 0.5, 0.25$ , and  $0$ , respectively. Three regimes exist,  $M_{\text{BH},6} < M_{\text{BH},6}^{\text{crit}}$ ;  $M_{\text{BH},6}^{\text{crit}} < M_{\text{BH},6} < M_{\text{BH},6}^{\text{warp}}$ , and  $M_{\text{BH},6} > M_{\text{BH},6}^{\text{warp}}$ . The knee at low BH masses shows the transition between the first and the second regime. The second transition is highlighted by the shaded vertical area (see text for details).

In this section we focus on the evolution of the spin magnitude  $a$  considering for the first time its coupling with the orientation  $\hat{\mathbf{J}}_{\text{BH}}$  and with the dynamical properties of the accretion.

Figure 5 shows the evolution of the BH spin  $a$  as a function of its mass, for the isotropic case and two different values of  $m_{\text{cloud}}$ . The memory of the initial spin is erased after the BH accretes a few times its initial mass ( $M_{\text{BH},0} = 10^4 M_{\odot}$ ), and  $a$  rises attaining values  $\approx 0.9$  during phase I. The large spin is a consequence of the rapid alignment induced by the Bardeen-Petterson

effect that occurs on a timescale  $\tau_{\text{al}} < \tau_{\text{acc}} < \tau_{\text{spin}}$  turning initially retrograde accretion into prograde accretion before disk consumption. Later, i.e. for larger BH masses, the spin drops to lower values, down to  $a \approx 0$ , for  $M_{\text{BH}} \gtrsim 10^9 M_{\odot}$ . The beginning of the spin decrease corresponds to the transition between phase I and II that occurs at different BH masses, depending on the value of  $m_{\text{cloud}}$ , as shown in the figure. The parameter that controls this transition is  $J_{\text{disc}}/J_{\text{BH}}$ : smaller clouds carry lower angular momenta and the transition between phase I and II occurs at smaller BH masses. The spin modulus decreases because over a single accretion episode

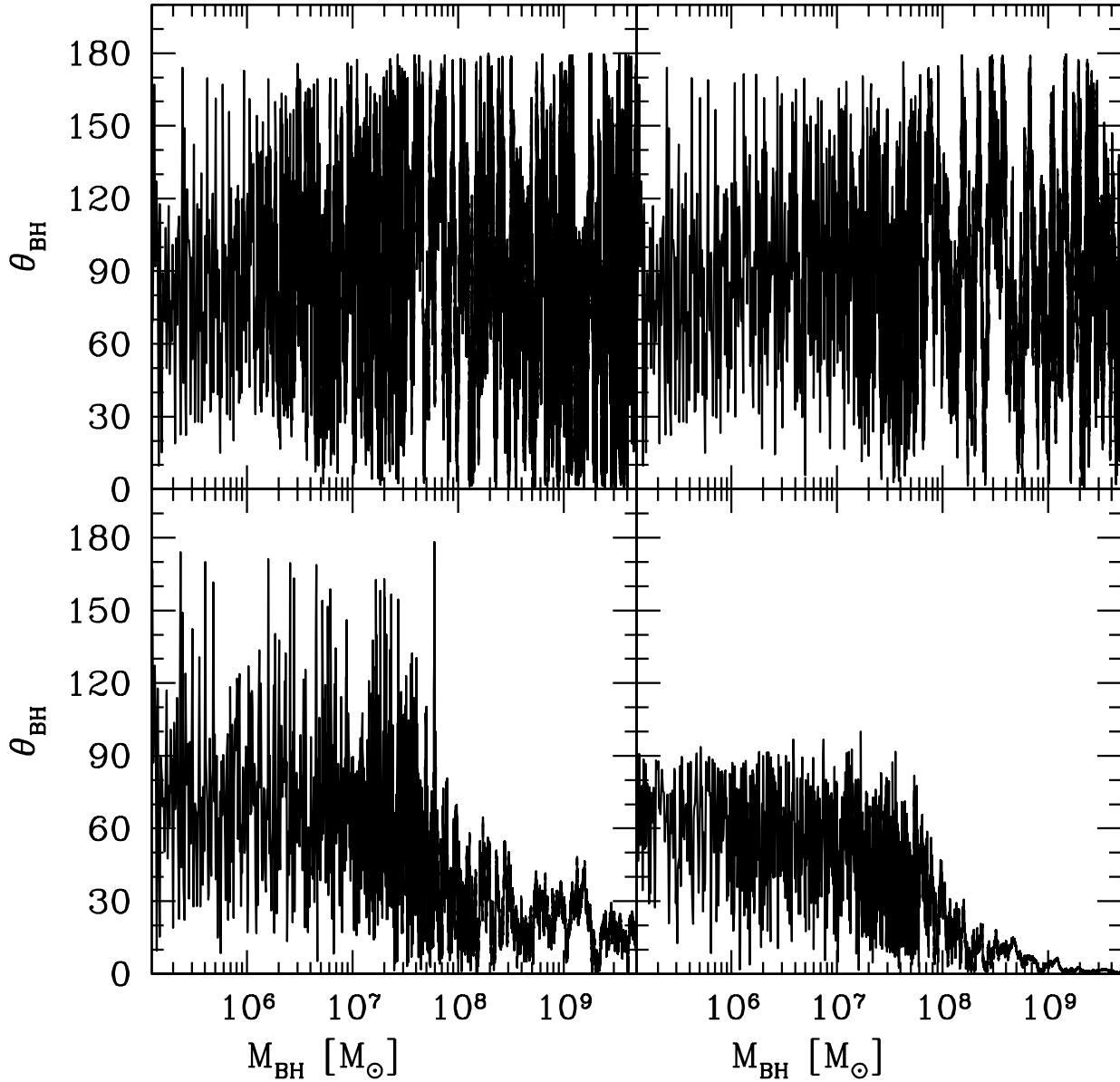


FIG. 3.— Evolution of the polar angle  $\theta_{\text{BH}}$  describing the BH spin orientation, relative to a fixed coordinate system, as a function of the BH mass. The upper left panel refers to the isotropic case ( $F = 0.5$ ) with a maximum mass per accretion event  $m_{\text{cloud}} = 10^4 M_{\odot}$ . The results in the upper right, lower left and lower right panels assume  $m_{\text{cloud}} = 10^5 M_{\odot}$  and  $F = 0.5, 0.25$ , and  $0$ , respectively.

$\hat{\mathbf{J}}_{\text{BH}}$  does not change significantly. Retrograde accretion episodes remain retrograde over the disk consumption timescale, so that, for isotropic fueling, the probability of having a prograde accretion events is exactly the same of having a retrograde one. Because the location of the ISCO is farther away, and therefore the accreted material carries a larger specific angular momentum, retrograde accretion transfers more angular momentum per unit mass than prograde accretion, isotropic fueling results in net spin-down and thus low spins (e.g. King & Pringle 2006).

Figure 6 shows the spin evolution for different value of the anisotropy parameter  $F = 0.5; 0.25; 0.125; 0$  (with

$m_{\text{cloud}} = 10^5 M_{\odot}$ ). The early phase (I) is similar in all the cases. Rapid BH-disk alignment results in  $a \approx 0.9$ . At the transition between phase I and II, the spin always decays, because at this transition the BH-disk alignment is only partial, and retrograde accretion is possible for a significant fraction of the time that elapses during each accretion event. By contrast, the value of the BH spin at large masses ( $M_{\text{BH}} \gtrsim 10^9 M_{\odot}$ ) is strongly dependent on the degree of anisotropy. For  $F = 0.25$ , large BHs carry spins with  $a \approx 0.45$ , and this asymptotic value of  $a$  increases with decreasing  $F$ . For  $F = 0$ , i.e. the highest degree of anisotropy described here,  $a \rightarrow 1$ . This is a consequence of the stability of the spin direction (discussed in section 3.1). For highly anisotropic cases, the massive



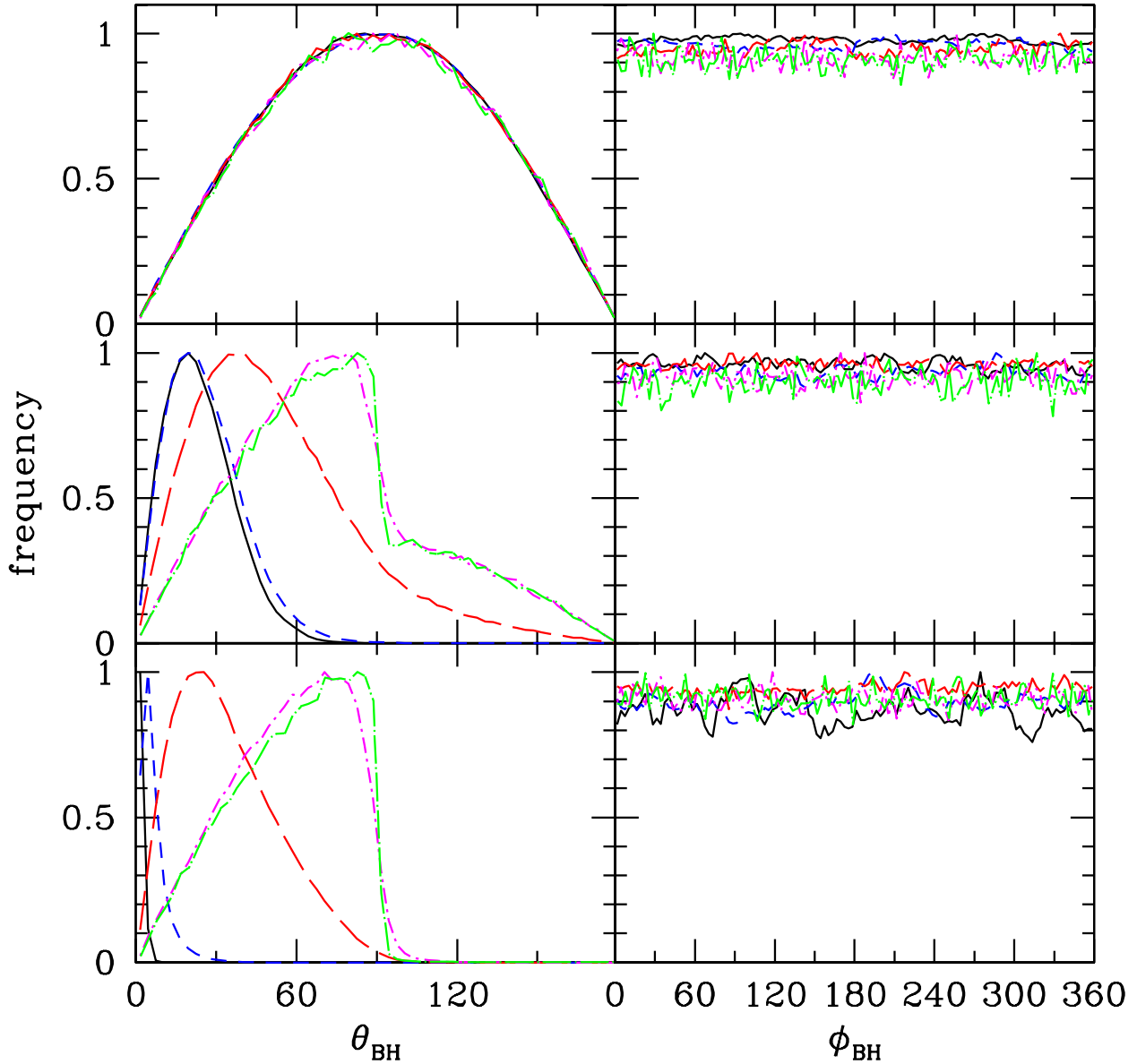


FIG. 4.— Distributions of the polar angle  $\theta_{\text{BH}}$  (left column) and azimuth angle  $\phi_{\text{BH}}$  (right column), for BHs of different masses, assuming  $m_{\text{cloud}} = 10^5 M_{\odot}$ . Top, middle, and bottom panels refer to the  $F = 0.5$ ,  $0.25$ , and  $0$  cases, respectively. BHs in the mass interval  $10^5 M_{\odot} - 10^6 M_{\odot}$  are denoted with green, long dot-dashed line,  $10^6 M_{\odot} - 10^7 M_{\odot}$  with purple, short dot-dashed line,  $10^7 M_{\odot} - 10^8 M_{\odot}$  with red, long-dashed line,  $10^8 M_{\odot} - 10^9 M_{\odot}$  with blue, short-dashed line, and  $> 10^9 M_{\odot}$  with black, solid line.

BHs tend to align their spins with the average angular momentum of the gas reservoir, resulting in an higher fraction of prograde accretion events. Thus, we can correlate the spin of the large BHs with the dynamics of the fueling mechanism.

Figure 7 shows the distribution of the BH spin in different mass intervals, assuming  $F = 0$  and  $m_{\text{cloud}} = 10^5 M_{\odot}$ . Here we emphasize that the highest spins are attained at the largest BH masses. The distribution corresponding to  $10^9 M_{\odot} < M_{\text{BH}} < 10^{9.5} M_{\odot}$  peaks at  $a \approx 0.997$ . This may have important implications on the efficiency at which these BHs can accrete, on the

statistics of very massive BHs, and on the possibility of launching jets (e.g. Tchekhovskoy & McKinney 2012). A large degree of anisotropy ( $F = 0$ ) is the only way to get maximally rotating BHs at the high mass end.

#### 4. COMPARISON WITH OBSERVATIONS

It is not straightforward to compare the predictions of our simple investigation with constraints on the BH masses and spins inferred from observations. Theoretically, a clear prediction of how the expected spin distribution evolves with the BH mass can be made once the distribution/dynamics of the fueling process is known (i.e., when  $F$  and  $m_{\text{cloud}}$  are known, in our context), and fuel-

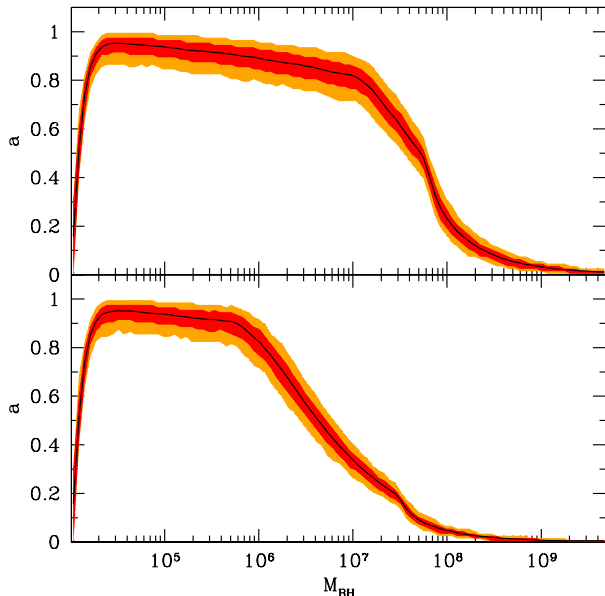


FIG. 5.— Evolution of the BH spin magnitude  $a$  as a function of  $M_{\text{BH}}$ , for the isotropic case ( $F = 0.5$ ). The upper (lower) panel refers to accretion episodes with  $m_{\text{cloud}} = 10^5 M_{\odot}$  ( $10^4 M_{\odot}$ ). The black line refers to the mean over 500 realizations. Red and orange shaded areas enclose intervals at  $1 - \sigma$  and  $2 - \sigma$  deviations, respectively.

ing can in principle differ depending on the galaxy types and masses. Observationally, the constraints on BH spins are often debated. However, we can make some very general comments on how our model fits within the observed trends. As discussed in the Introduction, the spin of a number of massive BHs has been measured through spectral fitting of the broad  $\text{K}\alpha$  iron lines at 6.4 keV. In almost all the cases, the measured spins are larger than 0.5, for BHs of masses  $10^6 M_{\odot} \lesssim M_{\text{BH}} \lesssim 10^8 M_{\odot}$ . The spin parameters of the BHs hosted in Swift J2127, NGC 3783, and MGC-6-30-15 are still debated, and could be lower than 0.5, with a minimum of  $a < 0.32$  for NGC 3783 (Patrick et al. 2011b, but see also Brenneman et al. 2011 for a higher estimate of  $a$ ). These measurements are in agreement with our simple model, i. e. there is always a history that can recover the observed spin for the mass observed. In particular these data suggest a non-negligible anisotropy in the fuelling of these BHs. Note however that this could be related to an observational bias toward measurements of highly spinning objects, as discussed in Brenneman et al. (2011).

A possible evolution of the BH spin with mass is found in the continuity-equation based study by Shankar, Weinberg & Miralda-Escudé (2011). In this study, a radiative efficiency (and as a consequence, a spin parameter) increasing with the BH mass is needed to avoid overproduction of BHs at the high mass end of the local observed mass function. A similar study by Li, Wang & Ho (2012) finds  $\eta$  increasing for increasing  $M_{\text{BH}}$  at high redshift ( $z \gtrsim 1$ ). We notice, however, that Li et al. do not recover this trend at low redshift. They found the radiative efficiency at  $z \lesssim 0.8$  to be almost independent on the BH mass. The accretion efficiency could be derived fitting observational data with accretion disk models for individual sources (Davis & Laor 2011; Raimundo

et al. 2012). However, the values determined are largely sensitive to the unknown parameters and uncertainties, which makes it very hard to draw any conclusions on the spin dependence with black hole mass, as discussed in Raimundo et al. (2012).

If the trend of  $\eta$  suggested by Shankar et al. (and by Li et al. for high redshifts) is confirmed, at least some massive BHs ( $M_{\text{BH}} \gtrsim 10^9 M_{\odot}$ ) must be very close to maximal rotation ( $a \gtrsim 0.98$ ), because of the very steep evolution of  $\eta$  close to  $a \approx 1$ . The dependence of  $\eta$  on  $a$  is quite sensitive as  $\eta$  varies from 0.151 for  $a = 0.90$ , to 0.43 for  $a = 1$ . BHs can be spun up to such high spins ( $a \gtrsim 0.98$ ) through BH-BH binary coalescences only when specific conditions on the spins of the parent BHs and the orbital configuration are met. A coalescing binary can result in a remnant BH with  $a \approx 1$  only if *i* the parent BHs were close to maximal rotation prior to merge, and had their spins aligned with the binary orbital angular momentum (Marronetti et al. 2008; Kesden et al. 2010a)<sup>7</sup>, *ii* through a long sequence of extremely unequal mergers all confined in the same well defined orbital plane (cf the “equatorial case” in Berti & Volonteri 2008). For coalescing BHs not rapidly rotating or with spins not aligned with their orbital angular momentum, the remnant is expected to have a smaller spin, with an average of  $a \sim 0.7$  (Hughes & Blandford 2003; Berti & Volonteri 2008). To summarize, BH coalescences can preserve high spins, but cannot be the original cause of extreme spins (Berti & Volonteri 2008). The reason for close-to-maximally rotating BHs must lie in their accretion history. The very large spins in the most massive BHs, if confirmed, will be an indication of a net degree of anisotropy in the fuelling of this objects ( $F \approx 0$ ). We note that our analysis predicts for the first time that the most rapidly rotating BHs ( $a > 0.98$ ) are also the most massive ones, and in addition, that the spin orientation is stable over many accretion cycles.

An independent constraint comes from jet observations. The bulk of luminous radio-loud AGN is associated with very massive BHs (e.g. McLure & Jarvis 2004; Metcalf & Magliocchetti 2006; Shankar et al. 2008a,b; Shankar et al. 2010) typically hosted in very massive ellipticals (e.g. Capetti & Balmaverde 2006). If the radio jet is powered by the extraction of rotational energy of the BHs, powerful radio sources would be related to rapidly rotating BHs (e.g. Blandford & Znajek 1977). Recent MHD simulations suggest that the power is a steep increasing function of the BH spin for  $a \sim 1$  (e.g. Tchekhovskoy & McKinney 2012, and references therein). In this scenario, our model predicts the most massive BHs to produce the most powerful jets, and jets are stable in their orientation if the BHs are not completely isotropically fueled (but not necessarily experience coherent accretion). The high mass BHs that have been fed by almost isotropically distributed gas have lower spins, and lower radio power. The difference in the fuelling process could explain the observed dichotomy of the radio-loudness of AGN (Sikora, Stawarz & Lasota 2007). The prediction of the most powerful jets being related to the most massive BHs is also in agreement with

<sup>7</sup> This configuration is predicted for gas rich galaxy mergers (Bogdanovic, Reynolds & Miller 2007; Dotti et al. 2010; Kesden et al. 2010b; Berti, Kesden & Sperhake 2012).

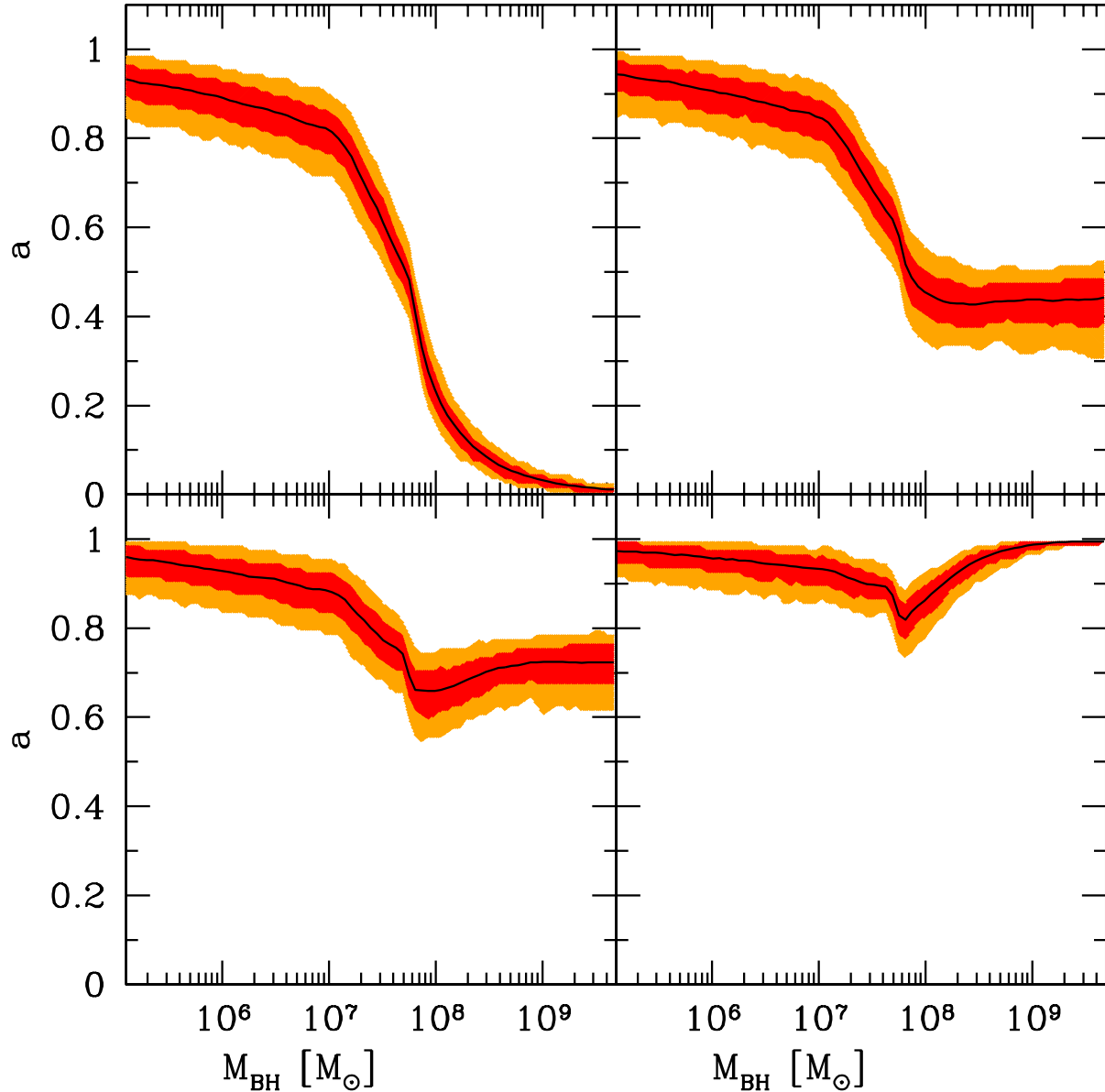


FIG. 6.— Evolution of the BH spin magnitude  $a$  as a function of  $M_{\text{BH}}$ , assuming  $m_{\text{cloud}} = 10^5 M_{\odot}$ . The upper left, upper right, lower left, and lower right panels refer to  $F = 0.5, 0.25, 0.125$ , and  $0$ , respectively. The colour code is as in figure 5.

the observed trend of the increasing fraction of radio-loud AGN for increasing BH masses (McLure et al. 1999; Jiang et al. 2007; Caccianiga et al. 2010; Chiaberge & Marconi 2011), and with the evidence that the most powerful radio and  $\gamma$ -loud AGN are associated to the heaviest supermassive BHs in the universe, with masses  $> 10^9 M_{\odot}$  (Ghisellini et al. 2010a,b).

We can also compare the distributions of the spin orientations for BHs of different masses as predicted by our model, with the observational constraints available to date. It is commonly accepted that the directions of relativistic jets in radio-loud AGN are not in a close correlation with the galaxy morphology (e.g. Schmitt et al. 2002; Verdoes Kleijn & de Zeeuw 2005). However, dif-

ferent degrees of alignment are observed, depending on the morphologies (and masses) of the host galaxies. Regarding Seyfert galaxies, the relative orientation of the jets and the minor axes of the galaxy is consistent with being drawn from an isotropic distribution (Clarke, Kinney & Pringle 1998; Nagar & Wilson 1999; Kinney et al. 2000). The degree of alignment seem to increase moving toward more massive galaxies and more massive BHs. Schmitt et al. (2002) studied the degree of misalignment between the direction of jets in radio-galaxies (early type and S0) and the direction normal to their nuclear disks, as traced by dust lanes. They found that the jets are typically misaligned with respect to the normal to the nuclear disks by less than  $55^{\circ} \sim 80^{\circ}$ . Similar re-

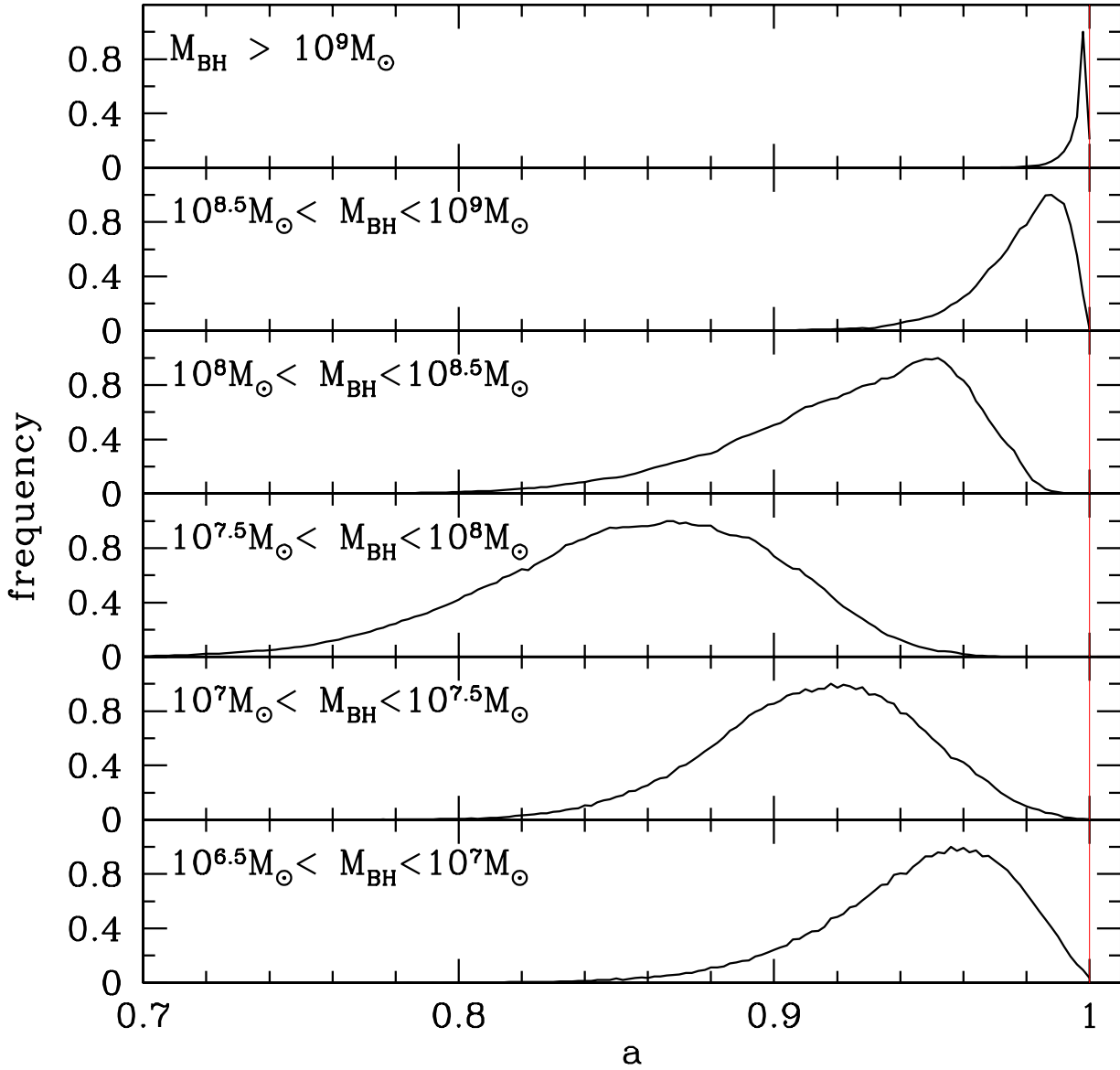


FIG. 7.— Distribution of the BH spin magnitude  $a$  for BHs in six different mass intervals, for  $F = 0$  and  $m_{\text{cloud}} = 10^5 M_{\odot}$ .

sults have been obtained by Verdoes Kleijn & de Zeeuw (2005) for low-power radio galaxies. They found slightly better alignments when comparing the direction of the jet and the normal to ellipsoidal-shaped dust lanes (tracers of nuclear disks), with a peak in the distribution of misalignments at  $\sim 45^\circ$ . Such a level of alignment is in contrast with an isotropic distribution, where a peak of misalignments is expected to coincide with the peak of the solid angle, at  $\sim 90^\circ$ . Note however that, given the uncertainties in the estimates, an isotropic distribution cannot be ruled out at more than the 95% confidence level (Verdoes Kleijn & de Zeeuw 2005). Verdoes Kleijn & de Zeeuw suggest that while dust ellipses trace gas on unperturbed Keplerian orbits that does not contribute to the fueling of the central AGN, dust lanes can bet-

ter trace perturbed gas that traces the material falling toward the BH. The degree of alignment between the normal to dust lanes and the jet direction is sensibly higher, with a peak of the distribution at  $20^\circ \sim 30^\circ$ . These studies suggest that a relation between jets and morphological properties of the galaxies exists only for massive galaxies, hosting massive BHs. This result is in broad agreement with our model (see Figure 4) that also indicates the stability of the jet direction, stability that is necessary to launch a large-scale jet, as seen in radio galaxies. We notice that on average the direction of the jet is expected to be related to the morphology of the nuclear distribution of gas, and not necessarily to the large scale stellar distribution. However, Saripalli & Subrahmanyan (2009) found that the largest radio sources (with

a projected linear size exceeding 700 kpc) have the jets preferentially aligned with the minor axes of their host galaxies. In the framework of our model, such a stable direction of very large scale jets can be explained if the BH is sufficiently massive ( $\gtrsim 10^9 M_\odot$ ), and hosted in a galaxy with a significant degree of anisotropy in its gas component. This trend is observed also by Browne & Battye (2010), as they observe ellipticals with a net rotation hosting jets preferentially aligned with the rotation axes, while non-rotating/triaxial ellipticals do not show such an alignment.

The predicted dependence of the magnitude and direction of  $J_{\text{BH}}$  on  $F$  can be further tested studying the nuclear gas dynamics around BHs with either an estimate of the spin parameter or a well constrained jet direction. Owing to its extreme angular resolution, the Atacama Large Millimeter/submillimeter Array is the likely to be instrumental in constraining the dynamics of dense molecular gas (and consequently  $F$ ) in the nuclei of nearby galaxies.

## 5. SUMMARY AND DISCUSSION

In this paper we explored the evolution of the spin parameter  $a$  (or  $J_{\text{BH}}$ ) of massive BHs considering the contemporary evolution of the orientation  $\hat{J}_{\text{BH}}$ , along sequences (histories) of accretion episodes. Histories are modeled as a succession of single accretion events where an  $\alpha$ -disk of given mass  $m_{\text{disk}}$  and orientation  $\mathbf{J}_{\text{disk}}$  forms. Disk orientation is not fixed but it is drawn from a distribution that carries a degree of anisotropy. This anisotropy is expected to be seeded in the gas clouds that surround the massive BH in the galactic nucleus and that are accreted. Our findings and their astrophysical consequences can be summarized as follows:

- At low BH masses ( $M_{\text{BH}} \lesssim 10^7 M_\odot$ ) the BH spin always aligns to the disk angular momentum in every single accretion episode, and can be substantially misaligned relatively to the average of the angular momenta of the disks. For  $M_{\text{BH}} \gtrsim 10^7 M_\odot$ , a single accretion episode does not modify significantly the BH spin direction. In this regime, the BH spin aligns with the average direction of the angular momentum of the accreting material, with a degree of alignment that increases with increasing anisotropy in the fueling process.
- *Small* BHs ( $M_{\text{BH}} \lesssim 10^7 M_\odot$ ) carry *large* spins  $a \sim 0.9$ . The *spin direction* changes *erratically* from episode to episode so that the vector  $\mathbf{J}_{\text{BH}}$  exhibits a random walk behavior, regardless the properties of the fueling process.
- *Large* BHs ( $M_{\text{BH}} \sim 10^9 M_\odot$ ) can carry either low spins or large spins, depending on the fueling conditions. The spin is low,  $a \approx 0$ , if the distribution of clouds in the hosts is *completely* random and isotropic. The spin is larger, up to  $a \gtrsim 0.99$ , and the *spin orientation* is *stable* on the sky *if* the gas accreting onto the central BH posses

some degree of anisotropy, i.e. *if* the accreting material has, on average, non zero angular momentum. Only if the degree of anisotropy is high ( $F = 0$ ) the most massive black holes can be maximally rotating.

- The most anisotropic case ( $F = 0$ ) studied here does not correspond to what is usually referred to as coherent accretion: for  $F = 0$ , two successive accretion events can be misaligned by up to 180 degrees.  $F = 0$  mimics accretion through disk clouds that are distributed isotropically but that share a common sense of rotation.  $F = 0$  corresponds to a 3D-dispersion to rotation velocity ratio  $\sigma/v_{\text{rot}} \lesssim 1$  for the gas fuelling the BH.
- There may exist an interval of BH masses, in between the two populations described above, in which the spins can be far from either zero or unity and changes orientation at random.
- Although our analysis predicts that most low mass BHs have substantial spins ( $a \sim 0.9$ ; see the two bottom panels of Figure 7), the most rapidly rotating BHs ( $a > 0.98$ ) are also the most massive ones (see upper panel of Figure 7). In addition, the spin orientation of the most massive BHs remains stable over many accretion cycles.
- The very large spins in the most massive BHs, if confirmed, will be an indication of a net degree of anisotropy in the fueling of this objects ( $F \approx 0$ ). In other words, our model predicts that a clear correlation exists between the kinematics of clouds feeding a BH and its spin, but only in the case of the most massive BHs ( $M_{\text{BH}} \gtrsim 10^7 M_\odot$ ).

As a final comment, we notice that light BHs ( $M_{\text{BH}} \lesssim 10^7 M_\odot$ ) carry large spins undergoing erratic changes in their orientation. This can have strong implications on the efficiency of feedback exerted by active BHs onto their host galaxy, that can potentially set the BH-host galaxy scale relations (see Nayakshin, Power & King 2012 and references therein). The higher "inertia" of the most massive BHs, if embedded in anisotropically moving gas, could reduce the feedback efficiency, since only a small solid angle would be affected. By contrast, if any anisotropic feedback (such as jets or biconical outflows, etc.) are launched during single episodes around less massive BHs, the spin random walk would result in a spread of the injected energy over  $4\pi$  during their lifetime.

Future studies will address the consequences of the model in the context of the cosmological evolution of BHs.

## ACKNOWLEDGMENTS

We thanks the anonymous Referee, Enrico Barausse, Alessandro Caccianiga, Francesco Haardt, Sandra Raimundo, Alberto Sesana, Francesco Shankar for comments and suggestions. MV acknowledges funding support from NASA, through award ATP NNX10AC84G; from SAO, through award TM1-12007X, and from a Marie Curie Career Integration grant (PCIG10-GA-2011-303609).

## REFERENCES

- Baker, J.G., Boggs, W.D., Centrella, J., Kelly, B.J., McWilliams, S.T., Miller, M.C., & van Meter, J.R., 2008, ApJ, 682, L29  
 Barausse, E., 2012, MNRAS, 423, 2533  
 Bardeen, J.M., 1970, Nature, 226, 64  
 Bardeen, J.M., Press, W.H., & Teukolsky, S.A. 1972, ApJ, 178, 347  
 Bardeen, J.M., & Petterson, J.A., 1975, ApJ, 195, L65  
 Berti, E., & Volonteri M., 2008, ApJ, 684, 822  
 Berti, E., Kesden, M., & Sperhake, U., 2012 (arXiv:1203.2920)  
 Blandford, R.D., & Znajek, R.L., 1977, 179, 433  
 Bogdanovic, T., Reynolds, C.S., & Miller, M.C., 2007, ApJ, 661, L147

- Brenneman, L.W., & Reynolds, C.S., 2006, *ApJ*, 652, 1028
- Brenneman, L.W., et al., 2011, *ApJ*, 736, 103
- Browne, I.W.A., & Battye, R.A., 2010, *ASPC*, 427, 365 (arXiv:1001.1409)
- Caccianiga, A., Severgnini, P., Della Ceca, R., & Corral, A., 2010, *ASPC*, 427, 389 (arXiv:0909.4165)
- Campanelli, M., Lousto, C.O., Zlochower, Y., & Merritt, D. 2007, *ApJ*, 659, L5
- Capetti, A., & Balmaverde, B., 2006, *A&A*, 453, 27
- Catinella, B., et al., 2010, *MNRAS*, 403, 683
- Chiaberge M. & Marconi A., 2011, *MNRAS*, 416, 917
- Clarke, C.J., Kinney, A.L., & Pringle, J.E., 1998, *ApJ*, 495, 189
- Davis, S.W., & Laor, A., 2011, *ApJ*, 728, 98
- de la Calle Perez, I., et al., 2010, *A&A*, 524, 50
- di Serego Alighieri, S. et al., 2007, *A&A*, 474, 851
- Dotti, M., Volonteri, M., Perego, A., Colpi, M., Ruszkowski, M., & Haardt, F., 2010, *MNRAS*, 402, 682
- Fanidakis, N., Baugh, C.M., Benson, A.J., Bower, R.G., Cole, S., Done, C., & Frenk, C.S., 2011, *MNRAS*, 410, 53
- Gallo, L.C., Miniutti, G., Miller, J.M., Brenneman, L.W., Fabian, A.C., Guainazzi, M., & Reynolds, C.S., 2011, *MNRAS*, 411, 607
- Ghisellini, G., Tavecchio, F., Foschini, L., Ghirlanda, G., Maraschi, L., & Celotti A., 2010a, *MNRAS*, 402, 497
- Ghisellini, G. et al., 2010b, *MNRAS*, 405, 387
- Gültekin, K. et al., 2009, *ApJ*, 698, 198
- Herrmann, F., Hinder, I., Shoemaker, D.M., Laguna, P., & Matzner, R. A., 2007, *Phys. Rev. D*, 76, 084032
- Hughes, S.A., & Blandford, R.D., 2003, *ApJ*, 585, L101
- Jiang, L., Fan, X., Ivezić, Z., Richards, G.T., Schneider, D.P., Strauss, M.A., & Kelly, B.C., 2007, *ApJ*, 658, 680
- Kesden, M., Lockhart, G., & Phinney, E.S., 2010a, *Phys. Rev D*, 82, 124045
- Kesden, M., Sperhake, U., & Berti, E., 2010b, *ApJ*, 715, 1006
- King, A.R., Lubow, S.H., Ogilvie, G.I., & Pringle, J.E., 2005, *MNRAS*, 363, 49
- King, A.R., & Pringle, J.E., 2006, *MNRAS*, 373, L90
- King, A.R., & Pringle, J.E., 2007, *MNRAS*, 374, L34
- King, A.R., Pringle, J.E., & Hofmann, J.A., 2008, *MNRAS*, 385, 1621
- Kinney, A.L., Schmitt, H.R., Clarke, C.J., Pringle, J.E., Ulvestad, J.S., & Antonucci, R.R.J., 2000, *ApJ*, 537, 152
- Kolykhalov, P. I., & Sunyaev, R. A., 1980, *Soviet Astronomy Letters*, 6, 357
- Li, Y.R., Wang, J.M., & Ho, L.C., 2012, *ApJ*, 749, L187
- Lodato, G., & Pringle, J.E., 2006, *MNRAS*, 368, 1196
- Lodato, G., & Pringle, J.E., 2007, *MNRAS*, 381, 1287
- Lousto, C.O., & Zlochower, Y., 2011, *Phys. Rev. L*, 107, 1102
- Lousto, C.O., Zlochower, Y., Dotti, M., & Volonteri, M., 2012, *Phys. Rev. D*, 85, 084015
- Marronetti, P. et al., 2008, *Phys. Rev. D*, 77, 064010
- Martin, R.G., Pringle, J.E., Tout, C.A., 2007, *MNRAS*, 381, 1617
- McConnell, N.J., et al. 2011, *Nature*, 480, 215
- McLure, R.J., Kukula M.J., Dunlop J.S., Baum S.A., O’Dea C.P., Hughes D.H., 1999, *MNRAS*, 308, 377
- McLure, R.J., & Jarvis, M.J., 2004, *MNRAS*, 353, L45
- Merritt, D., & Vasiliev, E. (arXiv:1208.6274)
- Metcalf, R.B., & Magliocchetti, M., 2006, *MNRAS*, 365, 101
- Nagar, N.M., & Wilson, A.S., 1999, *ApJ*, 516, 97
- Nayakshin, S., Power, C., & King, A.R., 2012, *ApJ*, 753, 15
- Patrick, A.R., Reeves, J.N., Lobban, A.P., Porquet, D., & Markowitz, A.G., 2011a, *MNRAS*, 411, 2353
- Patrick, A.R., Reeves, J.N., Lobban, A.P., Porquet, D., & Markowitz, A.G., 2011b, *MNRAS*, 416, 2725
- Perego, A., Dotti, M., Colpi, M., & Volonteri, M., 2009, *MNRAS*, 399, 2249
- Peterson, B.M., et al., 2005, *ApJ*, 632, 799
- Raimundo, S.I., Fabian, A.C., Vasudevan, R.V., Gandhi, P., & Jianfeng, W., 2012, *MNRAS*, 419, 2529
- Saripalli, L., & Subrahmanyam, R., 2009, *ApJ*, 695, 156
- Scheuer, P.A.G., & Feiler, R., 1996, *MNRAS*, 282, 291
- Schmitt, H.R., Pringle, J.E., Clarke, C.J., & Kinney, A.L., 2002, *ApJ*, 575, 150
- Schmoll, S. et al., 2009, *ApJ*, 703, 2171
- Schnittman, J.D., & Buonanno A., 2007, *ApJ*, 662, L63
- Schnittman, J.D., 2007, *ApJ*, 667, L133
- Shankar, F., Cavaliere, A., Cirasuolo, M., & Maraschi, L., 2008a, *ApJ*, 676, 131
- Shankar, F., Dai, X., & Sivakoff, G.R., 2008b, *ApJ*, 687, 859
- Shankar, F., Sivakoff, G.R., Vestergaard, M., & Dai, X., 2010, *MNRAS*, 401, 1869
- Shankar, F., Weinberg, D.H., & Miralda-Escudè, J., 2011 (arXiv:1111.3574)
- Shakura, N.I., & Sunyaev, R.A., 1973, *A&A*, 24, 337
- Sikora, M., Stawarz, L., & Lasota, J.P., 2007, *ApJ*, 658, 815
- Tchekhovskoy, A., & McKinney, J.C., 2012, *MNRAS*, 423, L55
- Verdoes Kleijn, G.A., & de Zeeuw, P.T., 2005, *A&A*, 435, 43
- Vestergaard, M., fan, X., Tremonti, C.A., Osmer, P.S., & Richards, G.T., 2008, *ApJ*, 674, L1
- Volonteri, M., 2007, *ApJ*, 663, L5
- Volonteri, M., Haardt, F., & Gültekin, K., 2008, *MNRAS*, 384, 1387
- Volonteri, M., Gültekin, K., & Dotti, M., 2010, *MNRAS*, 404, 2143